# 13C chemical shift map of the active cofactors in photosynthetic reaction centers of Rhodobacter sphaeroides revealed by photo-CIDNP MAS NMR

Prakash, S.; Alia, A.; Gast, P.; Groot, H.J.M. de; Jeschke, G.; Matysik, J.

# $^{13}$C Chemical Shift Map of the Active Cofactors in Photosynthetic Reaction Centers of *Rhodobacter sphaeroides* Revealed by Photo-CIDNP MAS NMR†

Shipra Prakash,‡,§ A. Alia,‡ Peter Gast,|| Huub J. M. de Groot,‡ Gunnar Jeschke,⊥ and Jörg Matysik*,‡

*Leiden Institute of Chemistry, P.O. Box 9502, 2300 RA Leiden, The Netherlands, Max-Planck-Institut für Bioanorganische Chemie, 45470 Mülheim/Ruhr, Germany, Leiden Institute of Physics, P.O. Box 9504, 2300 RA Leiden, The Netherlands, and Institut für Physikalische Chemie, Universität Konstanz, 78457 Konstanz, Germany*

*Received March 22, 2007; Revised Manuscript Received May 21, 2007*

ABSTRACT: $^{13}$C photo-CIDNP MAS NMR studies have been performed on reaction centers (RCs) of *Rhodobacter sphaeroides* wild type (WT) that have been selectively labeled with an isotope using [5-$^{13}$C]-*δ*-aminolevulinic acid·HCl in all the BChl and BPhe cofactors at positions C-4, C-5, C-9, C-10, C-14, C-15, C-16, and C-20. $^{13}$C CP/MAS NMR and $^{13}$C−$^{13}$C dipolar correlation photo-CIDNP MAS NMR provide a chemical shift map of the cofactors involved in the electron transfer process in the RC at the atomic scale. The $^{13}$C−$^{13}$C dipolar correlation photo-CIDNP spectra reveal three strong components, originating from two BChl cofactors, called P1 and P2 and assigned to the special pair, as well as one BPhe, $\Phi_A$. In addition, there is a weak component observed that arises from a third BChl cofactor, denoted P3, which appears to originate from the accessory BChl $B_A$. An almost complete set of assignments of all the aromatic carbon atoms in the macrocycles of BChl and BPhe is achieved in combination with previous photo-CIDNP studies on site-directed BChl/BPhe-labeled RCs [Schulten, E. A. M., Matysik, J., Alia, Kiihne, S., Raap, J., Lugtenburg, J., Gast, P., Hoff, A. J., and de Groot, H. J. M. (2002) *Biochemistry 41*, 8708−8717], allowing a comprehensive map of the ground-state electronic structure of the photochemically active cofactors to be constructed for the first time. The reasons for the anomaly of P2 and the origin of the polarization on P3 are discussed.



Photosynthesis in purple bacteria is driven by light-induced electron transfer in the reaction center (RC)[1] protein located in the intracytoplasmic membrane. The RC of *Rhodobacter sphaeroides* wild type (WT) is a transmembrane protein complex consisting of three polypeptide chains (H, M, and L) and 10 cofactors (*1*−*3*). Four BChl molecules ($P_L$, $P_M$, $B_A$, and $B_B$), two BPhe molecules ($\Phi_A$ and $\Phi_B$), two ubiquinones ($Q_A$ and $Q_B$), and a non-heme ferrous iron ($Fe^{2+}$) are arranged in two nearly symmetrical branches (Figure 1).

The tenth cofactor in *Rb. sphaeroides* WT is a carotenoid molecule (C), located near $B_B$, allowing for fast decay of electronic triplet states. The structural symmetry is in clear contrast to the functional asymmetry, which is a long-standing problem of structural biology (for a review, see ref *4*). The electron transfer takes place selectively via the active A-branch, while the B-branch is inactive for electron transfer. It is generally thought that the primary donor is the "special pair" (P), a dimer formed of the two strongly coupled BChl cofactors, $P_L$ and $P_M$. The primary acceptor is a BPhe molecule, $\Phi_A$. The remaining two accessory BChls, $B_A$ and $B_B$, are monomers. After photochemical excitation of P to P*, one electron is transferred to the primary electron

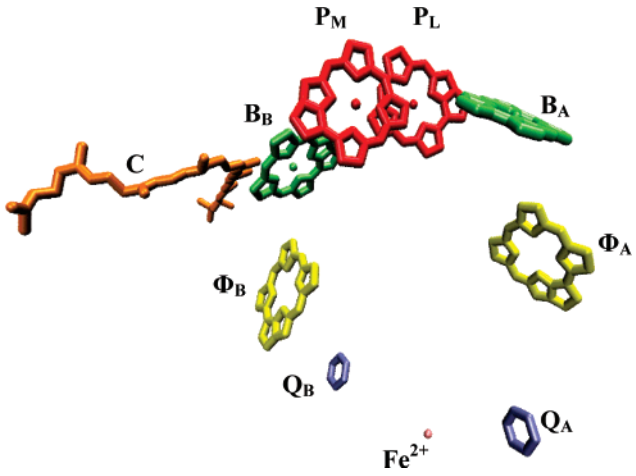


FIGURE 1: Detailed view of the cofactor arrangement in the RC of *Rb. sphaeroides* WT. The aliphatic chains from BChl, BPhe, and Q have been omitted for clarity.

† This work has been financially supported by the Netherlands Organization for Scientific Research (NWO) through a Jonge Chemici award (700.50.521), an Open competition grant (700.50.004), and a Vidi grant (700.53.423) as well as by the Volkswagen-Stiftung (I/78010) to J.M.

* To whom correspondence should be addressed. Telephone: +31-71-527-4198. Fax: +31-71-527-4603. E-mail: j.matysik@chem.leidenuniv.nl.

‡ Leiden Institute of Chemistry.

§ Max-Planck-Institut für Bioanorganische Chemie.

|| Leiden Institute of Physics.

⊥ Universität Konstanz.

[1] Abbreviations: 1D, one-dimensional; 2D, two-dimensional; ALA, *δ*-aminolevulenic acid; B, accessory bacteriochlorophyll; BChl, bacteriochlorophyll; BPhe or Φ, bacteriopheophytin; C, carotenoid; CP, cross polarization; DD, differential decay; DR, differential relaxation; LDAO, *N*,*N*-dimethyl dodecylamine-*N*-oxide; MAS, magic-angle spinning; P, special pair, primary electron donor; photo-CIDNP, photochemically induced dynamic nuclear polarization; PDSD, proton-driven spin diffusion; RC, reaction center; RFDR, radiofrequency-driven recoupling sequence; TSM, electron−electron−nuclear three-spin mixing; TPPM, two-pulse phase modulation; Q, ubiquinone; WT, wild type.

10.1021/bi700559b CCC: $37.00 
Published on Web 07/14/2007

acceptor $\Phi_A$ within 3 ps. In the next step, an electron is transferred to the primary quinone acceptor $Q_A$ in ~200 ps. Subsequently, an electron is transferred from $Q_A$ to the final acceptor $Q_B$. In quinone-depleted or quinone-reduced RCs, the forward transfer from BPhe to $Q_A$ is blocked, leading to the formation of the $P^{\bullet+}\Phi_A^{\bullet-}$ radical pair.

To determine the state in the electron transport in which the functional symmetry is broken, it has been proposed that the excited state P* is electronically asymmetric, having more electron density centered on $P_M$ (*5*). The electronic structure of the cation radical $P^{\bullet+}$ has been extensively investigated with EPR, ENDOR, and TRIPLE resonance studies (*6*−*8*). The studies have shown that the unpaired electron is unequally distributed over $P_L$ and $P_M$, favoring $P_L$ with a ratio of 2:1. This agrees well with photo-CIDNP MAS NMR investigations on RCs from *Rb. sphaeroides* (WT) reporting a ratio of electron spin density of 3:2 in favor of $P_L$ (*9*). On the other hand, the knowledge of P in the electronic ground state is limited. Resonance Raman studies suggested differences between $P_L$ and $P_M$ within the special pair (*10*, *11*). $^{15}N$ chemical shift data obtained via photo-CIDNP MAS NMR of uniformly $^{15}N$-labeled RCs show differences in the chemical shifts of the special pair cofactors (*12*−*14*), demonstrating that the symmetry within the special pair is already broken in the dark state. A more detailed view has been provided by $^{13}C$ photo-CIDNP MAS NMR on selective $^{13}C$ labeling (positions C-1, C-3, C-6, C-8, C-11, C-13, C-17, and C-19 in all porphyrin rings), suggesting that one of the cofactors in the special pair is distinguished (*15*).

Photochemically induced dynamic nuclear polarization (photo-CIDNP) magic-angle spinning (MAS) NMR is a method for studying the active cofactors in photosynthetic RCs with high sensitivity and selectivity (for reviews, see refs *16* and *17*). The chemical shift refers to the electronic ground state obtained after the photocycle, while the signal intensity is related to the local electron spin density. For the RCs from WT, photo-CIDNP has been described by a combination of two mechanisms (*16*). In the electron−electron−nuclear three-spin mixing (TSM) mechanism, net nuclear polarization is created in the spin-correlated radical pair due to the presence of both anisotropic hyperfine interaction and coupling between the two electron spins (*18*). In the differential decay (DD) mechanism, a net photo-CIDNP effect is caused by anisotropic hyperfine coupling without an explicit requirement for electron−electron coupling if spin-correlated radical pairs have different lifetimes in their singlet and triplet states (*19*). For both these mechanisms, the polarization after a single photocycle is roughly proportional to the square of the anisotropy of the hyperfine coupling and thus to the square of the electron spin density in $p_z$ orbitals on the observed nucleus. This allows for a mapping of electron densities in the radical pair state by analysis of NMR spectra of ground-state chromophores. Photo-CIDNP was observed for the first time in quinone-blocked bacterial RCs of *Rb. sphaeroides* R26 (*12*, *13*, *20*, *21*) and WT (*15*, *22*) using continuous illumination with white light, allowing an enhancement factor of ~200−1000. Furthermore, photo-CIDNP MAS NMR allowed for studies of the electronic structure of the cofactors involved into electron transfer in RCs of green sulfur bacteria (*23*) as well as of plant photosystem I (*24*) and photosystem II (*25*, *26*). A signal enhancement of a factor of 10,000 has been observed at a field strength of 4.7 T for both *Rb. sphaeroides* WT (*9*) and R26 (*27*). Due to the great enhancement of signal intensities, photo-CIDNP MAS NMR is not limited to isolated systems but has been applied to intact RCs in membrane-bound bacterial photosynthetic units (>1.5 MDa) (*28*) and in their cellular environement (*27*). In combination with site-directed $^{13}C$ labeling, photo-CIDNP MAS NMR is particularly powerful for the determination of the ground-state electronic structure of the cofactors involved in the electron transfer process with atomic selectivity. In this work, photo-CIDNP MAS NMR studies performed on selectively labeled BChl/BPhe RCs, labeled at positions C-4, C-5, C-9, C-10, C-14−C-16, and C-20, are reported. In combination with the previous paper (*15*), we present for the first time an almost complete set of $^{13}C$ chemical shifts of the aromatic systems of all active BChl and BPhe cofactors, allowing for a comprehensive map of the molecular electronic ground state of the photochemically active cofactors with atomic selectivity.

## MATERIALS AND METHODS

*Sample Preparation.* Cultures of *Rb. sphaeroides* WT (480 mL) were grown anaerobically in the presence of 1.0 mM [5-$^{13}C$]-*δ*-aminolevulinic acid·HCl ($COOHCH_2CH_2CO^{13}CH_2NH_2$·HCl, 99% $^{13}C$-enriched), purchased from Cambridge Isotope Laboratories (Andover, MD). Incorporation of [5-$^{13}C$]-ALA, as reported in this paper, produces BChl and BPhe macrocycles, labeled at C-4, C-5, C-9, C-10, C-14−C-16, and C-20 (Figure 2). The cultures were grown for 7 days in light. Before the cells were harvested for the preparation of RCs, a 4 mL aliquot was taken from the culture and the extent of $^{13}C$ incorporation of [4-$^{13}C$]ALA into BChl was determined as described in detail previously (*15*). The total level of incorporation of the $^{13}C$ label in BChl/BPhe ($^{13}C_{0-8}$) was 60 ± 5%. The culture was centrifuged for 10 min at 5500*g*, and the combined pellet was resuspended in 0.1 M phosphate buffer (pH 7.5). The RCs were isolated as described in ref *29*. Approximately 15 mg of the selectively labeled RC was reduced with 0.5 M sodium dithionite and used for the NMR experiments.

*MAS NMR Measurements.* Photo-CIDNP MAS NMR experiments were performed with a DMX-200 NMR spectrometer equipped with a double-resonance MAS probe operating at 200 MHz for $^1H$ and 50 MHz for $^{13}C$. The RC sample was loaded into an optically transparent 4 mm sapphire rotor, and $^{13}C$ MAS NMR spectra were recorded at a temperature of 223 K with a spinning frequency of 8 kHz. The sample was illuminated continuously during the course of the experiment. The illumination setup has been described in detail elsewhere (*17*, *21*). 1D photo-CIDNP MAS NMR spectra were collected with a Hahn echo-pulse sequence and two-pulse phase modulation (TPPM) proton decoupling (*30*). A recycle delay of 4 s was used. $^{13}C$ cross-polarization MAS NMR data were obtained with an AV-750 NMR spectrometer. A total of 4K scans were recorded at a temperature of 223 K with a spinning frequency of 12 kHz. For the 2D homonuclear ($^{13}C-^{13}C$) dipolar correlation spectra, adapted radiofrequency-driven recoupling (RFDR) and proton-driven spin diffusion (PDSD) pulse sequences were applied. The initial cross-polarization step in these pulse sequences was replaced by a $\pi/2$ pulse. The RFDR experiments were recorded with mixing times of 4 and 8 ms. The

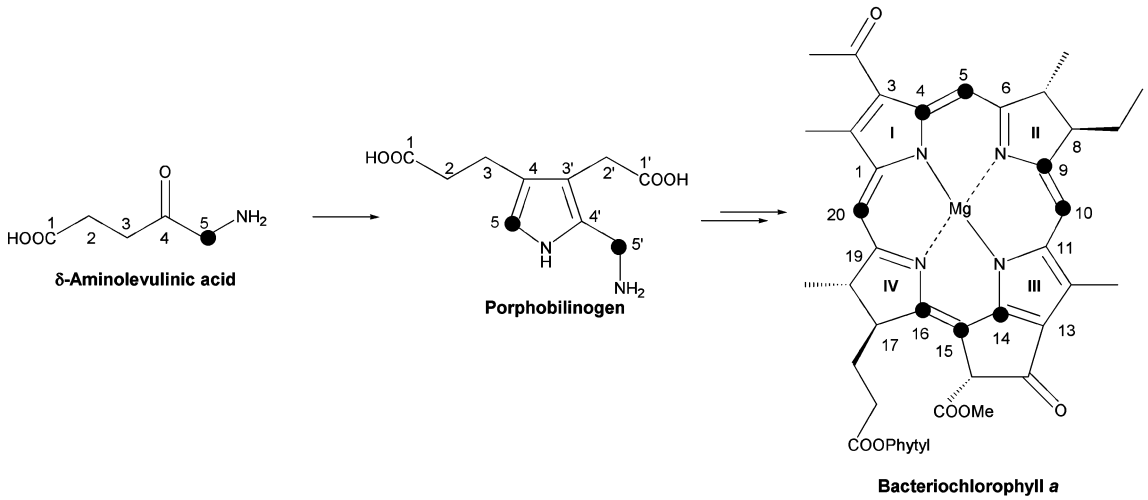


FIGURE 2: Schematic representation of the biosynthesis of BChl *a* and BPhe *a* starting from δ-aminolevulinic acid (ALA). The positions of $^{13}C$ labels are indicated with filled circles (●). The numbering of BChl *a* is according to the IUPAC nomenclature.

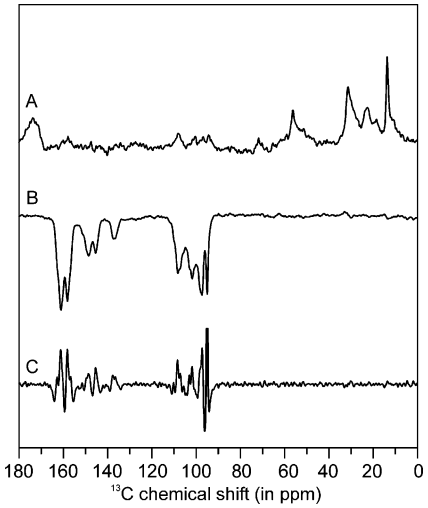


FIGURE 3: 1D solid-state MAS NMR spectra of the BChl/BPhe-labeled RC of *Rb. sphaeroides* WT. The dark $^{13}C$ CP/MAS NMR spectrum (A) was recorded at a field strength of 17.6 T at 223 K with a spinning frequency of 12 kHz. The photo-CIDNP spectrum (B) was recorded with continuous illumination in white light at a field strength of 4.7 T and 223 K with a spinning frequency of 8 kHz. Spectrum C is the second derivative of the 1D photo-CIDNP spectrum (B).

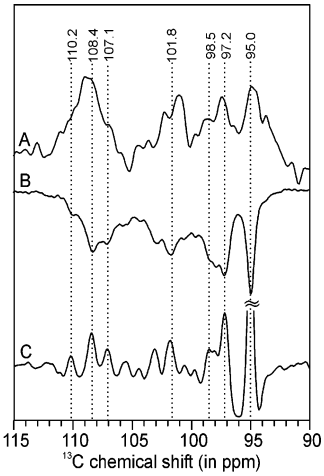


FIGURE 4: Detailed view of the methine region in the spectra in Figure 3. In both light and dark spectra, the labeled carbons resonate with comparable chemical shifts, visualized by dotted lines.

PDSD experiments were recorded with mixing times of 10 ms, 500 ms, and 1 s. In the $t_2$ dimension, 2K data points with a sweep width of 50 kHz were recorded. Zero filling to 4K and an exponential line broadening of 25 Hz were applied prior to Fourier transformation. In the $t_1$ dimension, 256 scans using 1K data points were recorded. A sine-squared apodization shifted by $\pi/2$ was applied prior to Fourier transformation. All spectra were externally referenced to the $^{13}$COOH response of solid tyrosine·HCl at 172.1 ppm.

## RESULTS AND DISCUSSION

*Comparison of Light with Dark Spectra.* The $^{13}C$ CP/MAS NMR spectrum from labeled RCs obtained in the dark is shown in Figure 3A. Several broad $^{13}C$ responses are observed between 10 and 70 ppm from the saturated carbons in the protein. The signal at 173 ppm is due to the amide carbonyl carbons of the protein. Weak signals are observed in the region from 90 to 110 ppm, corresponding to the responses of the methine carbons of BChl and BPhe cofactors which are selectively enriched with $^{13}C$. Continuous illumination with white light generates the photo-CIDNP MAS NMR spectrum shown in Figure 3B. Strong emissive peaks appear in the region between 90 and 110 ppm due to the photo-CIDNP of methine atoms $^{13}$C-5, $^{13}$C-10, $^{13}$C-15, and $^{13}$C-20. In the aromatic region of the spectrum from 135 to 165 ppm, the responses of $^{13}$C-4, $^{13}$C-9, $^{13}$C-14, and $^{13}$C-16 are detected. To separate the responses of the various labeled carbons, the second derivative of the 1D photo-CIDNP spectrum (Figure 3B) of the labeled RCs was calculated as shown in Figure 3C. There are photo-CIDNP signals from more than eight carbons, demonstrating that more than one BChl produced photo-CIDNP polarization. The broad peaks at 108.4, 97.2, and 95.2 ppm in the $^{13}C$ CP/MAS spectrum (Figure 3A) are narrower and strongly emissive in the photo-CIDNP spectrum (Figure 3B). These peaks are resolved better by taking the second derivative of the 1D photo-CIDNP spectrum (Figure 3C).

A detailed view of the spectra from 90 to 115 ppm is shown in Figure 4. In experiments conducted under continuous illumination, the RC is observed mainly in a light-adapted state leading to longer radical-pair lifetimes (*31*).

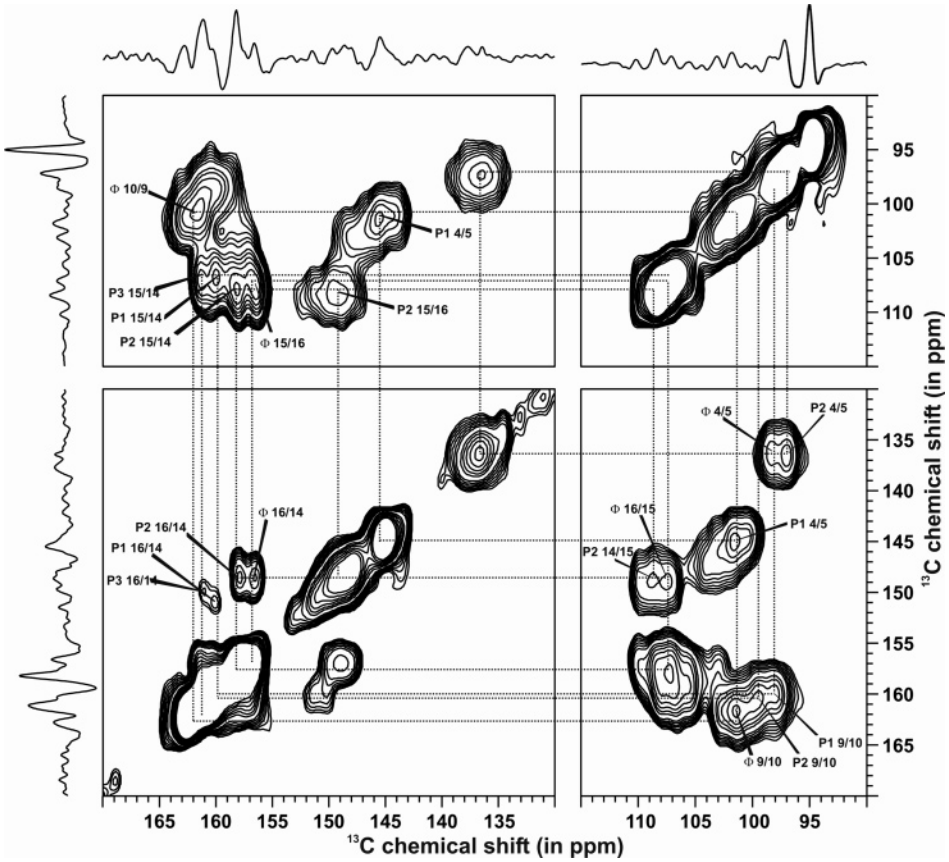


FIGURE 5: Contour plot sections of a $^{13}C-^{13}C$ dipolar correlation photo-CIDNP MAS NMR spectrum of [$^{13}C_{0-8}$]BChl/BPhe-labeled RCs of *Rb. sphaeroides* WT recorded at a field strength of 4.7 T and 223 K, using a spinning frequency of 8 kHz and a mixing time of 4 ms. The labels refer to the cross-peaks for the three BChl components (P1, P2, and P3) and the BPhe component (Φ). The top trace shows parts of the second derivative of the 1D photo-CIDNP MAS NMR spectrum.

In the experiments described here, no hints of light-induced changes in the ground-state electronic structure of the cofactors are obtained. Hence, conformational switching between dark- and light-adapted sample states is not linked to a large change in the ground-state electronic structure of the cofactors. Since earlier studies (*15*, *32*) found evidence that the vicinity of the donor cofactors is very rigid, these light-induced changes may be caused by soft structural elements such as hydrogen bonds.

*Assignment of the $^{13}C-^{13}C$ Dipolar Correlation Spectra.* To gain information about the ground-state electronic structure of the donor, P, and the acceptor molecule, Φ, 2D photo-CIDNP RFDR data sets were collected from polarized samples. The RFDR spectrum (Figure 5) was recorded with a mixing time of 4 ms. In the BChl and BPhe rings separated by a single bond, strong correlations appear within each pair of enriched carbons, i.e., C-4/C-5, C-9/C-10, C-14/C-15, and C-15/C-16. In addition, cross-peaks are observed between C-14 and C-16 over a distance of ∼2.3 Å. Four sets of correlation networks are visible. Three components which give strong correlations are assigned to two BChl molecules denoted P1 and P2 and one is assigned to BPhe, $\Phi_A$. The fourth component is weaker and is assigned to a third BChl cofactor, denoted P3.

The NMR shifts from BChl *a* and BPhe *a* molecules in solution are listed in Table 1. The methine carbons in BChl *a* and BPhe *a* in acetone-$d_6$ resonate between 95 and 110 ppm, and the chemical shift differences of the methine carbons between BChl and BPhe are ≤2 ppm. In contrast, C-4, C-9, C-14, and C-16 have much larger chemical shift differences. Hence, the diagonal peaks in the region from 95 to 110 ppm are attributed to C-5, C-10, C-15, and C-20 of the BChl and BPhe cofactors, forming the starting point of the assignment procedure. The $^{13}C$ responses for C-14 and C-16 of Φ in acetone-$d_6$ at 148.7 and 158.7 ppm, respectively, overlap with C-16 and C-14 of BChl at 152.2 and 160.8 ppm, respectively. Three correlations are observed

Table 1: Chemical Shifts of Monomeric BChl *a* and BPhe *a* Cofactors

| | BChl *a* | | | | BPhe *a* | |
|---|---|---|---|---|---|---|
| carbon | $\sigma_{liq}$[a] | P1[b] | P2[b] | P3[b] | $\sigma_{liq}$[a] | Φ[b] |
| 1 | 150.8 | 148.2 | 143.4 | 148.5 | 139.7 | 138.3 |
| 3 | 137.4 | 130.2 | 127.6 | 133.2 | 134.8 | 134.7 |
| 4 | 150.2 | 145.4 | 136.8 | | 138.1 | 136.8 |
| 5 | 99.6 | 101.6 | 97.2 | | 98.4 | 98.4 |
| 6 | 168.4 | 166.8 | 164.6 | 167.0 | 170.9 | 171.1 |
| 8 | 55.6 | 53.0 | 55.4 | 50.6 | 55.4 | 54.6 |
| 9 | 158.5 | 160.2 | 161.0 | | 164.3 | 162.2 |
| 10 | 102.4 | 98.1 | 99.6 | | 100.4 | 101.5 |
| 11 | 149.4 | 150.3 | 154.2 | 149.4 | 139.3 | 138.9 |
| 13 | 130.3 | 131.0 | 131.3 | 130.2 | 129.3 | 126.4 |
| 14 | 160.8 | 160.0 | 158.0 | 161.2 | 148.7 | 149.1 |
| 15 | 109.7 | 106.8 | 108.2 | 107.1 | 109.9 | 107.5 |
| 16 | 152.2 | 151.4 | 148.8 | 150.3 | 158.7 | 156.6 |
| 17 | 50.4 | 47.3 | 49.7 | 48.7 | 51.5 | 52.5 |
| 19 | 167.1 | 162.5 | 159.7 | 162.7 | 169.8 | 169.9 |
| 20 | 96.3 | | 94.5 | | 97.6 | 94. |

[a] The liquid NMR chemical shift data ($\sigma_{liq}$) were obtained in acetone-$d_6$. [b] Assignments for C-1, C-3, C-6, C-8, C-11, C-13, C-17, and C-19 from ref *15*.

for C-14/C-15 at 160.0/106.8 ppm (P1), 158.0/108.2 ppm (P2), and 161.2/107.1 ppm (P3). A correlation is also observed for C-16/C-15 of Φ at 149.1/107.5 ppm. In addition, correlations are observed for C-16/C-15 of P2 at 148.8/108.2 ppm and C-14/C-15 of Φ at 149.1/107.5 ppm. These assignments are confirmed by cross-peaks detected between C-14 of ring III and C-16 of ring II. Two strong correlations are observed for C-14/C-16 at 158.0 /148.8 ppm (P2) and for C-16/C-14 at 149.1/156.6 ppm (Φ). Furthermore, two weak correlations are observed for C-14/C-16 at 160.0/151.4 ppm (P1) and at 161.2/150.3 ppm (P3). A correlation is observed for C-9/C-10 of Φ at 162.2/101.5 ppm. The $^{13}$C response from C-9 of BChl overlaps with the $^{13}$C response of C-14 of BChl. Cross-peaks observed between C-9/C-10 of P2 at 161.0/99.6 ppm and of P1 at 160.2/98.1 allow for assignment to C-9. Finally, correlations are detected at 136.8/98.4 ppm and at 136.8/97.2 ppm. The $^{13}$C response for C-4 of Φ in acetone-$d_6$ is at 138.1 ppm, and hence, the peak at 136.8/97.2 ppm is assigned to C-4/C-5 of Φ. There is another C-4/C-5 correlation observed which cannot be assigned to a Φ, since only one Φ is present in the active branch. Since the $^{13}$C response of C-5 of BChl in acetone-$d_6$ is at 99.6 ppm, this can be assigned to a C-4/C-5 correlation of BChl. Thus, the C-4/C-5 correlation at 136.8/98.4 ppm is assigned to P2. Finally, a correlation is observed at 145.4/101.6 ppm. This correlation can be assigned to C-4/C-5 of a BChl since it is nearer to the $^{13}$C response of C-4 of BChl at 150.2 ppm. Thus, it is assigned to C-4/C-5 of P1. RFDR experiments performed with a mixing time of 8 ms did not show any additional peaks.

PDSD experiments performed with a mixing time of 500 ms show significantly more peaks as compared to the RFDR experiment with a mixing time of 4 ms (Figure 6). Cross-peaks are now observed between C-20 and the carbons around it. Peaks are thus observed for P2 between C-14/C-20, C-16/C-20, and C-4/C-20. Correlations are also observed between C-16/C-10 and methine carbons like C-15/C-10 and C-15/C-20 of P2. A few cross-peaks are also observed for carbons of $\Phi_A$ like C-5/C-14, C-20/C-14, and C-10/C-14. There are two weak peaks observed which can be assigned to intermolecular carbons between P2 and P1. These are between P1 C-5/P2 C-14 and P1 C-4/P2 C-5 over a distance of 3−7 Å.

The complete list of the $^{13}$C assignments for all the photochemically active cofactors is presented in Table 1. Since no correlations were observed between C-9/C-10 or C-4/C-5 for P3, it was not possible to complete these assignments. Upfield shifts are observed for several carbons of P1, P2, and P3. The chemical shift differences ($\Delta\sigma = \sigma_{ss} - \sigma_{liq}$) for the three BChls (P1, P2, and P3) and one BPhe ($\Phi_A$) are shown in Figure 7. To build a comprehensive map of the electronic ground-state structure of the photochemically active cofactors, $^{13}$C assignments from previous photo-CIDNP MAS NMR studies (*15*) are also included in Table 1 and Figure 7. With both label patterns, the same global pattern is observed: (i) three correlation networks of BChls and one of a BPhe, (ii) two BChl networks with strong and one with weak intensity, and (iii) among the two strong BChl correlation networks, one significantly more different from a BChl in solution. Both those correlation networks with a maximum $\Delta\sigma$ of both label patterns were called P2.

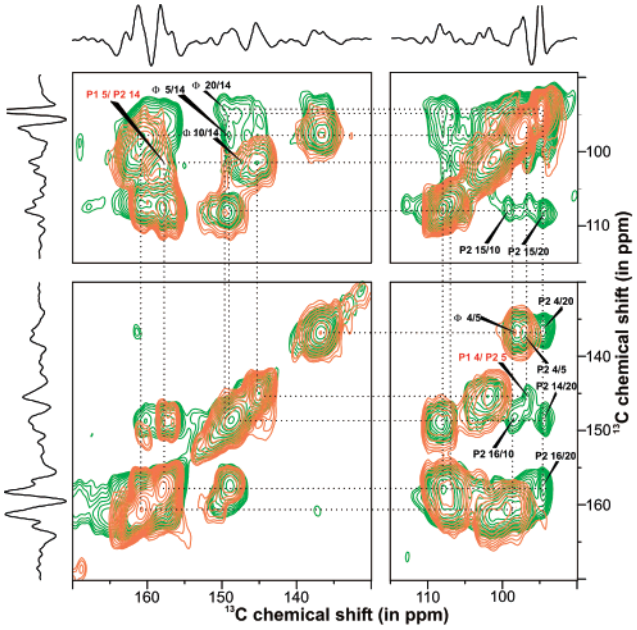


FIGURE 6: Contour plot sections of a $^{13}$C−$^{13}$C dipolar correlation photo-CIDNP MAS NMR spectra of [$^{13}C_{0-8}$]BChl/BPhe-labeled RCs of *Rb. sphaeroides* WT, recorded at a field strength of 4.7 T and 223 K using a spinning frequency of 8 kHz. The RFDR spectrum (orange) recorded with a mixing time of 4 ms is overlaid on the PDSD spectrum (green) recorded with a mixing time of 500 ms. The labels refer to the cross-peaks for the three BChl components (P1, P2, and P3) and the BPhe component (Φ), and the numbers refer to the IUPAC numbering of carbons for the chlorophyll ring. Assignments to intermolecular peaks are colored red. The top trace shows parts of the second derivative of the 1D photo-CIDNP MAS NMR spectrum.

The BPhe $\Phi_A$ cofactor exhibits both upfield and downfield shifts of <3 ppm, except for C-4 which shows an upfield shift of 4.8 ppm. In BChls P1, P2, and P3, the carbons around rings I and IV are shifted upfield compared to other carbons. Pronounced upfield shifts are observed especially for P2 in pyrrole ring I as compared to P1 and P3. This effect is clearly visible in C-1, C-3, and C-4 of P2, which are shifted upfield by 7.4, 9.8, and 13.4 ppm, respectively. On the other hand, for P1 and P3, carbons around rings I and IV are shifted upfield by 2−7 ppm. The two BChls, $P_L$ and $P_M$, of P overlap over ring I. Ring current shifts may be considered as an explanation of the strong upfield shifts around ring I for P2. However, ring current shifts which are upfield in the range of only 1−3 ppm have been observed for porphyrins (*33*, *34*) and cannot therefore explain shifts in the range of 7−13 ppm. Furthermore, ring current shifts are expected to be symmetrical. Hence, comparison of the chemical shifts of the three BChl cofactors suggests that one of them is distinguished, which is called P2.

*Identity of the Cofactors.* The pronounced upfield shifts in ring I of P2 suggest strong interactions in its vicinity of other cofactors, which are the other BChl cofactor in P (either $P_L$ or $P_M$) and $B_A$. Furthermore, there are several polar amino acid residues surrounding the cofactors. The large upfield shifts could be explained by a strong interaction like a hydrogen bond to one of the amino acid residues. The X-ray structure of the RC reveals that a histidine residue (His L168) is within hydrogen bonding distance of the 3-acetyl group of $P_L$ (Figure 8) (*1*). Resonance Raman studies provide further evidence that a hydrogen bond exists at the 3-acetyl

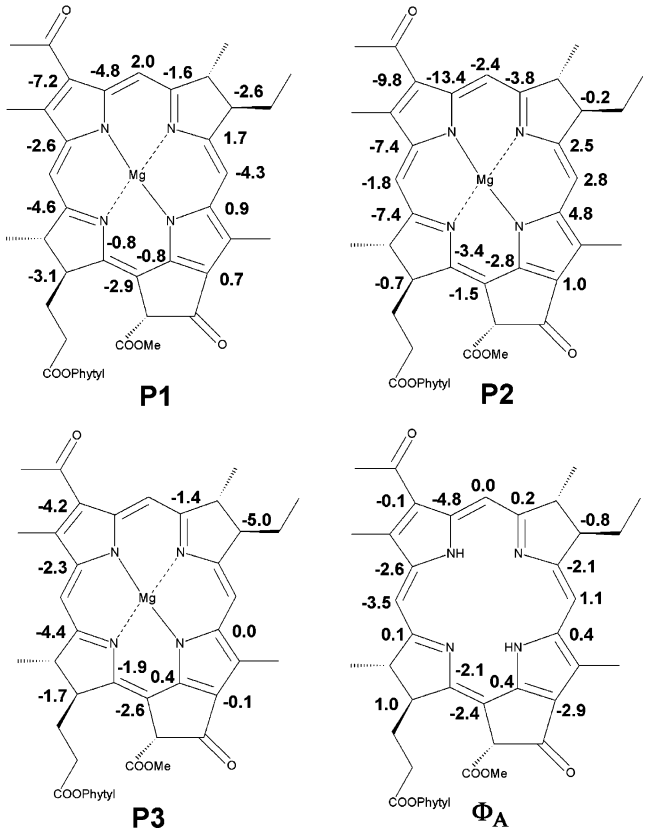


FIGURE 7: Detected chemical shift differences ($\Delta\sigma = \sigma_{ss} - \sigma_{liq}$) for the three BChls (P1, P2, and P3) and the BPhe ($\Phi_A$). The positive values denote an upfield shift and the negative values a downfield shift.

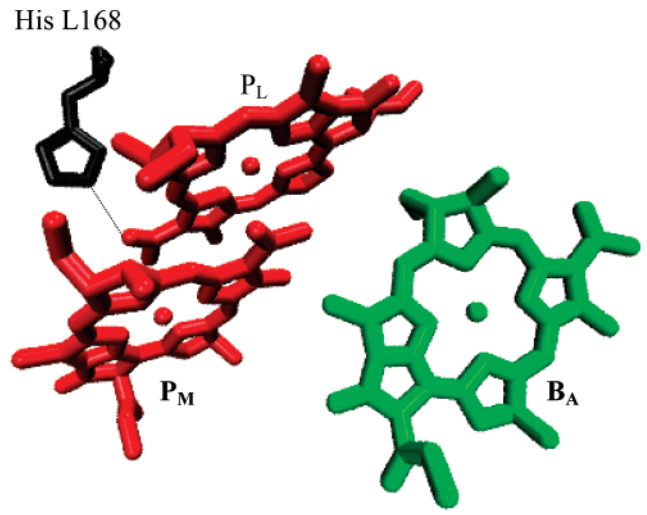


FIGURE 8: Side view of the special pair, $P_L$ and $P_M$, and front view of the accessory BChl $B_A$. His L168 in the back interacts with the 3-acetyl group of $P_L$.

group of $P_L$ (*10*). In addition, site-directed mutants at positions His L168 and Phe M197 show that the occurrence of a hydrogen bond can be correlated with an increase in the dimer midpoint potential (*35*). Hence, the appearance of the strong upfield shifts in ring I of P2 can be assigned to the hydrogen bonding between the acetyl carbonyl and the NH group of the imidazole side chain of His L168. This would lead to the assignment of P2 to $P_L$ which in the BChl cofactor of P is located at the active A-branch. Therefore, the other strong BChl component P1 is assigned to $P_M$, and the weak component P3 is assigned to the accessory BChl in the active branch, $B_A$.

The different chemical shifts of $P_L$ in comparison to those of $P_M$ and $B_A$ indicate a special local electronic environment in the ground state around $P_L$. The upfield shift of 13.4 ppm at C-4 of $P_L$ indicates a stabilization of approximately −0.08 electronic equivalent negative charge per atom relative to the monomeric solution (*36*). Strong upfield shifts around ring I of $P_L$, and to a lesser extent around ring IV, suggest a distribution of the electronic charge over these rings primarily. The role of His L168 may be the stabilization of the charge on $P_L$. The comprehensive map of the electronic ground state of the special pair presented here confirms previous results (*15*) which showed that P is asymmetric already in the electronic ground state with excess negative charge on $P_L$. The functional asymmetry in the RC is thus introduced in the ground state.

*Involvement of Accessory BChl $B_A$.* An assignment of P3 to a disturbed special pair cofactor is unlikely since such a strong disturbance would hardly affect only a single cofactor of the special pair. The assignment of the weak BChl component, P3, to the accessory BChl cofactor $B_A$ raises the question of the mechanism producing enhanced nuclear polarization. The involvement of an accessory BChl $B_A$ molecule as a real intermediate in the electron transfer to $\Phi_A$ has been a matter of debate (for a review, see ref *4*). Absorbance difference spectroscopy with femtosecond time resolution did not elucidate any involvement of $B_A$ (*37*). On the other hand, other transient femtosecond measurements yielded a biphasic kinetics which could be interpreted as only a two-step model of electron transfer, suggesting the involvement of $B_A$ (*38*−*40*). From subpicosecond transient measurements, it has been suggested that both the two-step hopping and the one-step superexchange model of ET may coexist (*41*). There has also been the suggestion of a pathway of electron transfer that does not involve the excited state of the special pair dimer (P*) but instead is driven by the excited state of the monomeric BChl ($B_A$*) (*42*). An alternative interpretation based on spin couplings can bring about electron transfer from P* to $P^{\bullet+}\Phi_A^{\bullet-}$ with the involvement of a triplet−triplet−singlet $^TB^TB_A$ as an intermediate between the excited charge-separated P* state and the primary charge-separated $P^+\Phi_A^-$ state (*43*). In all those concepts, however, the involvement of $B_A$ is too short-lived to generate primary nuclear polarization on $B_A$, since processes driven by hyperfine interaction require durations of at least some tens of nanoseconds. On the other hand, buildup of nuclear polarization by spin diffusion would be expected to affect partially also the accessory BChl cofactor of the inactive branch ($B_B$). Such a possibility would imply that both accessory BChl cofactors have very similar chemical shift patterns. Another possibility is that $B_A$ might substitute for one of the chlorophylls in $P^{\bullet+}$; i.e., there might be a fraction of special pairs that involve, besides the "distinguished" chlorophyll P2, the accessory chlorophyll $B_A$ instead of P1. Alternatively, it might be possible that the cation radical spin density is distributed over the special pair and the accessory chlorophyll $B_A$.

## CONCLUSION

From the aromatic systems of both cofactors of the special pair, an almost complete set of $^{13}C$ chemical is presented. Cofactor $P_L$ of the active branch, assigned to P2, is the BChl showing most significant differences to a BChl in chloroform. Especially dramatic chemical shift changes appear on pyrrole ring I which may be due to hydrogen bonding interaction of the C-3′ carbonyl with a histidine of the protein pocket. Hence, the electronic structure of two BChl cofactors, $P_L$ and $P_M$, forming the special pair in RCs of *Rb. sphaeroides* is already distinguished in their electronic ground state, and the break of symmetry between the cofactors is already present in dark RCs. The primary acceptor BPhe appears to be relatively undisturbed.

## ACKNOWLEDGMENT

The help of F. Lefeber, J. G. Hollander, and K. Erkelens is gratefully acknowledged. We thank A. de Wit for his help in sample preparation. S.P. thanks Prof. W. Lubitz for his kind help and support.

## REFERENCES

1. Ermler, U., Fritzsch, G., Buchanan, S. K., and Michel, H. (1994) Structure of the photosynthetic reaction center from *Rhodobacter sphaeroides* at 2.65-Å resolution: Cofactors and protein-cofactor interactions, *Structure 2*, 925−936.
2. Yeates, T. O., Komiya, H., Chirino, A., Rees, D. C., Allen, J. P., and Feher, G. (1988) Structure of the reaction center from *Rhodobacter sphaeroides* R26 and 2.4.1-protein-cofactor (bacteriochlorophyll, bacteriopheophytin, and carotenoid) interactions. 4, *Proc. Natl. Acad. Sci. U.S.A. 85*, 7993−7997.
3. Camara-Artigas, A., Brune, D., and Allen, J. P. (2002) Interactions between lipids and bacterial reaction centers determined by protein crystallography, *Proc. Natl. Acad. Sci. U.S.A. 99*, 11055−11060.
4. Hoff, A. J., and Deisenhofer, J. (1997) Photophysics of photosynthesis, *Phys. Rep. 287*, 2−247.
5. Moore, L. J., Zhou, H. L., and Boxer, S. G. (1999) Excited-state electronic asymmetry of the special pair in photosynthetic reaction center mutants: Absorption and stark spectroscopy, *Biochemistry 38*, 11949−11960.
6. Lendzian, F., Huber, M., Isaacson, R. A., Endeward, B., Plato, M., Bönigk, B., Möbius, K., Lubitz, W., and Feher, G. (1993) The electronic-structure of the primary donor cation-radical in *Rhodobacter sphaeroides* R26: ENDOR and triple-resonance studies in single-crystals of reaction centers, *Biochim. Biophys. Acta 1183*, 139−160.
7. Rautter, J., Lendzian, F., Lubitz, W., Wang, S., and Allen, J. P. (1994) Comparative study of reaction centers from photosynthetic purple bacteria: Electron paramagnetic resonance and electron nuclear double resonance spectroscopy, *Biochemistry 33*, 12077−12084.
8. Lubitz, W., Lendzian, F., and Bittl, R. (2002) Radicals, radical pairs and triplet states in photosynthesis, *Acc. Chem. Res. 35*, 313−320.
9. Prakash, S., Alia, Gast, P., de Groot, H. J. M., Jeschke, G., and Matysik, J. (2005) Magnetic field dependence of photo-CIDNP MAS NMR on photosynthetic reaction centers of *Rhodobacter sphaeroides* WT, *J. Am. Chem. Soc. 127*, 14290−14298.
10. Mattioli, T. A., Hoffmann, A., Robert, B., Schrader, B., and Lutz, M. (1991) Primary donor structure interactions in bacterial reaction centers from near-infrared fourier-transform resonance Raman spectroscopy, *Biochemistry 30*, 4648−4654.
11. Palaniappan, V., Martin, P. C., Chynwat, V., Frank, H. A., and Bocian, D. F. (1993) Comprehensive resonance Raman study of photosynthetic reaction centers from *Rhodobacter sphaeroides*: Implications for pigment structure and pigment-protein interactions, *J. Am. Chem. Soc. 115*, 12035−12049.
12. Zysmilich, M. G., and McDermott, A. (1994) Photochemically induced dynamic nuclear-polarization in the solid-state $^{15}N$ spectra of reaction centers from photosynthetic bacteria *Rhodobacter sphaeroides* R26, *J. Am. Chem. Soc. 116*, 8362−8363.
13. Zysmilich, M. G., and McDermott, A. (1996) Photochemically induced nuclear spin polarization in bacterial photosynthetic reaction centers: Assignments of the $^{15}N$ SSNMR spectra, *J. Am. Chem. Soc. 118*, 5867−5873.
14. Prakash, S., Tong, S., Alia, Gast, P., de Groot, H. J. M., Jeschke, G., and Matysik, J. (2004) in *Photosynthesis: Fundamental Aspects to Global Perspectives* (van der Est, A., and Bruce, D., Eds.) pp 236−238, Allen Press, Montreal.
15. Schulten, E. A. M., Matysik, J., Alia, Kiihne, S., Raap, J., Lugtenburg, J., Gast, P., Hoff, A. J., and de Groot, H. J. M. (2002) $^{13}C$ MAS NMR and photo-CIDNP reveal a pronounced asymmetry in the electronic ground state of the special pair of *Rhodobacter sphaeroides* reaction centers, *Biochemistry 41*, 8708−8717.
16. Jeschke, G., and Matysik, J. (2003) A reassessment of the origin of photochemically induced dynamic nuclear polarization effects in solids, *Chem. Phys. 294*, 239−255.
17. Daviso, E., Jeschke, G., and Matysik, J. (2006) Photochemically Induced Dynamic Nuclear Polarization Magic-Angle Spinning NMR, in *Biophysical Methods in Photosynthesis II* (Aartsma, T. J., and Matysik, J., Eds.) Chapter 19, Springer-Verlag, Dordrecht, The Netherlands.
18. Jeschke, G. (1998) A new mechanism for chemically induced dynamic nuclear polarization in the solid state, *J. Am. Chem. Soc. 120*, 4425−4429.
19. Polenova, T., and McDermott, A. E. (1999) A coherent mixing mechanism explains the photoinduced nuclear polarization in photosynthetic reaction centers, *J. Phys. Chem. B 103*, 535−548.
20. Zysmilich, M. G., and McDermott, A. (1996) Natural abundance solid-state carbon NMR studies of photosynthetic reaction centers with photoinduced polarization, *Proc. Natl. Acad. Sci. U.S.A. 93*, 6857−6860.
21. Matysik, J., Alia, Hollander, J. G., Egorova-Zachernyuk, T., Gast, P., and de Groot, H. J. M. (2000) A set-up to study photochemically induced dynamic nuclear polarization in photosynthetic reaction centres by solid-state NMR, *Indian J. Biochem. Biophys. 37*, 418−423.
22. Matysik, J., Alia, Gast, P., Lugtenburg, J., Hoff, A. J., and de Groot, H. J. M. (2001) Photochemically induced dynamic nuclear polarization observed in bacterial photosynthetic reaction centers observed by $^{13}C$ solid state NMR, *Focus Struct. Biol. 1*, 215−225.
23. Roy, E., Alia, Gast, P., van Gorkom, H. J., de Groot, H. J. M., Jeschke, G., and Matysik, J. (2007) Photochemically induced dynamic nuclear polarization in the reaction center of the green sulphur bacterium *Chlorobium tepidum* observed by $^{13}C$ MAS NMR, *Biochim. Biophys. Acta 1767*, 610−615.
24. Alia, Roy, E., Gast, P., van Gorkum, H. J., de Groot, H. J. M., Jeschke, G., and Matysik, J. (2004) Photochemically Induced Dynamic Nuclear Polarization in Photosystem I of Plants Observed by $^{13}C$ Magic-Angle Spinning NMR, *J. Am. Chem. Soc. 126*, 12819−12826.
25. Matysik, J., Alia, Gast, P., van Gorkom, H. J., Hoff, A. J., and de Groot, H. J. M. (2000) Photochemically induced nuclear spin polarization in reaction centers of photosystem II observed by $^{13}C$ solid-state NMR reveals a strongly asymmetric electronic structure of the $P^{\bullet+}_{680}$ primary donor chlorophyll, *Proc. Natl. Acad. Sci. U.S.A. 97*, 9865−9870.
26. Diller, A., Alia, Roy, E., Gast, P., van Gorkom, H. J., de Groot, H. J. M., Zaanen, J., Glaubitz, C., and Matysik, J. (2005) Photo-CIDNP solid-state NMR on photosystems I and II: What makes P680 special? *Photosynth. Res. 84*, 303−304.
27. Prakash, S., Alia, Gast, P., de Groot, H. J. M., Matysik, J., and Jeschke, G. (2006) Photo-CIDNP MAS NMR in intact cells of *Rhodobacter sphaeroides* R26: Molecular and atomic resolution at nanomolar concentration, *J. Am. Chem. Soc. 128*, 12794−12799.
28. Prakash, S., Alia, Gast, P., Jeschke, G., de Groot, H. J. M., and Matysik, J. (2003) Photochemically Induced Dynamic Nuclear polarisation in entire bacterial photosynthetic units observed by C-13 magic-angle spinning NMR, *J. Mol. Struct. 661*, 625−633.
29. Shochat, S., Arlt, T., Francke, C., Gast, P., Vannoort, P. I., Otte, S. C. M., Schelvis, H. P. M., Schmidt, S., Vijgenboom, E., Vrieze, J., Zinth, W., and Hoff, A. J. (1994) Spectroscopic characterization of reaction centers of the (M)Y210W mutant of the photosynthetic bacterium *Rhodobacter sphaeroides*, *Photosynth. Res. 40*, 55−66.
30. Bennett, A. E., Rienstra, C. M., Auger, M., Lakshmi, K. V., and Griffin, R. G. (1995) Heteronuclear decoupling in rotating solids, *J. Chem. Phys. 103*, 6951−6958.

31. van Mourik, F., Reus, M., and Holzwarth, A. R. (2001) Long-lived charge-separated states in bacterial reaction centers isolated from *Rhodobacter sphaeroides*, *Biochim. Biophys. Acta 1504*, 311−318.
32. Fischer, M. R., de Groot, H. J. M., Raap, J., Winkel, C., Hoff, A. J., and Lugtenburg, J. (1992) $^{13}$C magic-angle spinning NMR study of the light-induced and temperature-dependent changes in *Rhodobacter sphaeroides* R26 reaction centers enriched in 4′-$^{13}$C tyrosine, *Biochemistry 31*, 11038−11049.
33. Giessner-Prettre, C., and Pullman, B. (1971) Molecular Orbital Calculations on Conformation of Polypeptides and Proteins. 7. Refined Calculations on Alanyl Residue, *J. Theor. Biol. 31*, 287−294.
34. Stolzenberg, A. M., Simerly, S. W., Steffey, B. D., and Haymond, G. S. (1997) The synthesis, properties, and reactivities of free-base- and Zn(II)-N-methyl hydroporphyrin compounds. The unexpected selectivity of the direct methylation of free-base hydroporphyrin compounds, *J. Am. Chem. Soc. 119*, 11843−11854.
35. Lin, X., Murchison, H. A., Nagarajan, V., Parson, W. W., Allen, J. P., and Williams, J. C. (1994) Specific alteration of the oxidation potential of the electron donor in reaction centers from *Rhodobacter sphaeroides*, *Proc. Natl. Acad. Sci. U.S.A. 91*, 10265−10269.
36. Tokuhiro, T., and Fraenkel, G. (1969) Origin of Linearity of Carbon-13 Shift with Charge. Calculations for Azines, *J. Am. Chem. Soc. 91*, 5005−5013.
37. Martin, J. L., Breton, J., Hoff, A. J., Migus, A., and Antonetti, A. (1986) Femtosecond spectroscopy of electron transfer in the reaction center of the photosynthetic bacterium *Rhodopseudomonas sphaeroides* R26: Direct electron transfer from the dimeric bacteriochlorophyll primary donor to the bacteriopheophytin acceptor with a time constant 2.8 ± 0.2 psec, *Proc. Natl. Acad. Sci. U.S.A. 83*, 957−961.
38. Holzapfel, W., Finkele, U., Kaiser, W., Oesterhelt, D., Scheer, H., Stilz, H. U., and Zinth, W. (1989) Observation of a bacteriochlorophyll anion radical during the primary charge separation in a reaction center, *Chem. Phys. Lett. 160*, 1−7.
39. Holzapfel, W., Finkele, U., Kaiser, W., Oesterhelt, D., Scheer, H., Stilz, H. U., and Zinth, W. (1990) Initial electron transfer in the reaction center from *Rhodobacter sphaeroides*, *Proc. Natl. Acad. Sci. U.S.A. 87*, 5168−5172.
40. Holzwarth, A. R., and Müller, M. G. (1996) Energetics and kinetics of radical pairs in reaction centers from *Rhodobacter sphaeroides*. A femtosecond transient absorption study, *Biochemistry 35*, 11820−11831.
41. Chan, C. K., Dimagno, T. J., Chen, L. X. Q., Norris, J. R., and Fleming, G. R. (1991) Mechanism of the initial charge separation in bacterial photosynthetic reaction centers, *Proc. Natl. Acad. Sci. U.S.A. 88*, 11202−11206.
42. van Brederode, M. E., van Mourik, F., van Stokkum, I. H. M., Jones, M. R., and van Grondelle, R. (1999) Multiple pathways for ultrafast transduction of light energy in the photosynthetic reaction center of *Rhodobacter sphaeroides*, *Proc. Natl. Acad. Sci. U.S.A. 96*, 2054−2059.
43. Fischer, S. F., and Scherer, P. O. J. (1997) Charge separation in photosynthesis via a spin exchange coupling mechanism, *Eur. Biophys. J. 26*, 477−483.

BI700559B